WIRE INSULATION FLAMMABILITY EXPERIMENT: USML-1

1 YEAR POST MISSION SUMMARY

Paul S. Greenberg*, Kurt R. Sacksteder* and Takashi Kashiwagi+

*NASA Lewis Research Center, Cleveland, OH
+National Institute of Standards and Technology, Gaithersburg, MD.

ABSTRACT

Herein we report the results from the Wire Insulation Flammability (WIF) Experiment performed in the Glovebox Facility on the USML-1 mission. This experiment explored various aspects of electrically induced fire scenarios in a reduced gravity environment. Under quiescent microgravity conditions, heat and mass transfer are dominated by diffusive and radiative transport; while in normal-gravity buoyancy-induced convection often dominates. Of considerable scientific and practical interest is the intermediate situation of combustion occurring in the presence of imposed gas flows, with lower characteristic velocities than those induced by buoyancy in normal gravity. Two distinct cases naturally arise: flow direction opposed to, or concurrent with, the flame spread direction. Two tests of each kind were conducted in the WIF experiment, providing the first controlled demonstration of flame spreading in forced convection ever conducted in space.

Four test modules were flown. The wire insulation, 1.5 mm in diameter, was polyethylene, extruded onto nichrome wire. Temperatures of the wire cores and insulation heated in quiescent and flowing environments were measured. Video and still-camera images of the samples, burning in air flowing at approximately 10 cm/sec, were recorded to obtain flame characteristics including spread rate, structure and temperature. Flame spread rates in concurrent flow were approximately twice those in opposed flow.

Several unexpected and unique microgravity combustion phenomena were observed. In concurrent and opposed flow regimes, the spreading flames stabilized around a bead of molten insulation material, within which bubble nucleation was observed. An ignition attempt without flow created a quiescent cloud of vaporized fuel which ignited dramatically yet failed to sustain normal flame spread. Finally, all tests produced substantial soot agglomerates, particularly the concurrent flow tests; and the collected soot has a morphology very distinct from soot formed in normal gravity flames.

Joint "L+1" Science Review for USML-1 and USMP-1 with the Microgravity Measurement Group, September 22-24, 1993, Huntsville, Alabama, USA.

INTRODUCTION

Combustion is a ubiquitous phenomenon that affects nearly everyone in some way either as an energy source for cooking, heating, transportation, electrical power generation, and a variety of industrial processes, or as a destructive agent in fires. Some people believe civilization began when mankind conceived the concept of controlling fire, yet after thousands of years uncontrolled fires still cause tremendous injury and property damage. Because of its importance to modern civilization, combustion has been the object of scientific study for over a century. Still, many questions remain to be answered.

Convection plays a role in most combustion phenomenon, providing the necessary oxidizer and affecting the chemical reaction rates and the distribution of the heat released in the flame. In normal gravity, buoyant convection introduces additional complexity: the heat released in the flame induces the density gradient upon which gravity acts to induce flow. Some normal gravity flames are completely dominated by buoyant convection, even though convection would cease without that flame.

Flame spreading tests have been conducted using thin fuels in microgravity situations, where buoyant convection is suppressed. In spacecraft experiments, (e.g. the Solid Surface Combustion Experiment[1]) flames were ignited in quiescent atmospheres with an elevated oxygen content. These tests demonstrated diffusional mechanisms can be sufficient alone to sustain flame spreading. In ground-based facilities (i.e. drop towers and parabolic aircraft) convection at very low speeds has sustained flames at much lower concentrations of atmospheric oxygen[2,3,4] than quiescent microgravity tests similarly configured. The ground-based tests, however, were limited to very thin fuels (e.g. tissue paper); practical fuels, which are thicker, require more test time than is available. One objective of the Wire Insulation Flammability Experiment was to obtain the first extended observations of low-speed convection in flames spreading over fuels resembling engineering materials.

The WIF experiment also provided an opportunity to conduct a simple heat transfer experiment. On Earth, buoyant convection plays a role in the disposition of heat generated by resistance (joule) heating in electrical wires. Ratings for the current carrying capacity of wires rely partially upon buoyant convective cooling to dissipate the energy of joule heating. Similarly, the cooling of electrical components is commonly accomplished using finned heat-sink structures that also rely upon buoyant cooling. In microgravity buoyant convection is suppressed, and electrical systems in spacecraft are cooled by other means (e.gs. cold plates, forced convection, heat exchangers, and heat conducted through the wires). Joule heating rates in quiescent and very-low-speed flows were measured with the WIF experiment for comparison with tests in normal-gravity buoyant environments.

I. EXPERIMENTAL OBJECTIVES

The Wire Insulation Flammability Experiment (WIF) was designed to obtain test data on two related phenomena:

(1) Observe and measure the joule heating of electrical wire in a quiescent, then low-speed forced-flow environments, for comparison with normal-gravity behavior and with established tests for rating spacecraft electrical systems.

(2) Observe and measure the ignition and spreading of a flame over the insulation of overheated electrical wire in very-low-speed flows in microgravity. Distinguish between flames spreading in concurrent and opposed flow, and compare with flame spreading in normal gravity.

To obtain these desired observations, four experiments were conceived, two each in concurrent and opposed flows.

II. EXPERIMENT HARDWARE

Four nearly-identical WIF test modules, designated WIF-A,B,C, and D (see figure 1) were built for the STS-50 mission. The modules were designed to function inside the Glovebox Experiment Facility (GBX) which provided electrical power, flowing air, and photographic capability.

Each module consisted of a combustion chamber (see figure 2) open at both ends, configured as a miniature wind tunnel. At one end a flexible duct was provided for connection to the GBX air circulation system, the air supply for the experiment. A small bending flag anemometer, made from the jewel-bearing movement of an electrical meter, was positioned in the tunnel to indicate the airflow velocity. A metal screen covered the exit port to cool the gases exiting the WIF module and to contain any particulates released during combustion.

A single insulated wire sample, 1.5 mm diameter, 110 mm long, was mounted axially in the duct, parallel to the airflow direction. The sample consisted of polyethylene insulation extruded onto a 0.75 mm nichrome wire core. The sample was connected to circuitry design to provide current for joule heating the nichrome core. At one end of the sample, a kanthol igniter wire was wound around the insulation. In two modules, the ignitor was located near the flow exit so that the flame spread direction would be opposed to the airflow direction; in the others, the ignitor was located near the entrance for concurrent-flow flame spreading.

The electrical power deposited in the test wire cores via joule heating was controlled by calibrated ballast resistors. The power deposition in the WIF modules A-D were 1.27, 1.49, 1.59, and 1.75 watts, respectively. The resistances were selected to achieve different steady temperatures in the wire samples near the melting point of the insulation, based on tests in a vacuum in normal gravity.

Four Type K, 0.07 mm wire diameter thermocouples were placed inside the sample to measure wire temperatures and insulation temperatures near, but below, the surface. Two additional thermocouples were located in the gas phase, 2.5 mm and 1.5 mm from the insulation surface, to

measure the flame temperatures. A window in the tunnel was framed by six thermocouple-temperature displays (see figure 2). This window configuration was designed to allow simultaneous imaging of the flame and the thermocouple displays using the glovebox video. A second window in the tunnel presented an orthogonal perspective used for 35 mm still photographs.

Two 10 cc vacuum bottles, located behind the combustion chamber, were connected through a solenoid valve to small-diameter metal sampling tubes, that terminated near the wire sample. The vacuum bottles were designed for collecting gaseous samples of the off-gassing and combustion products for post-flight chemical analysis. Two transmission electron microscope grids, approximately 3 mm in diameter, were attached to each exit screen for post-flight analysis of any captured particles.

The crew controlled the WIF modules using a small control box outside the GBX. The controlled functions included: wire heating, ignition, and gas sampling (2 samples per module). The control functions were actuated with momentary switches to prevent inadvertant overheating, etc.

III. EXPERIMENT OPERATIONS

Following installation of a test module and the photography devices, and establishing electrical connections, the nominal test procedures were a sequence of crew actions for wire heating then ignition. The first phase of the experiment consisted of recording temperatures of the sample during preheating - first in a quiescent (no-flow) environment. The crew member was to actuate the electrical current flow, stopping when the predetermined insulation temperature was reached. The first of two gas samples were to be taken at this time. Next, the airflow was to be activated and adjusted using observations of the anemometer. The wire heating was then to be repeated in the convective cooling regime.

When the wire insulation reached a predetermined temperature, the crew member was to terminate the wire heating and then activate the ignitor. Upon observing ignition, the crew member was to deactivate the ignitor and trigger the motor-driven still camera. During the spreading of the flame, the second vacuum bottle was to be momentarily opened for collecting a sample of the combustion products. Video images of the temperature displays and the spreading flame were to be recorded throughout the heating and burning processes.

IV. TEST RESULTS AND DISCUSSION

A. SAMPLE PREHEATING

Electrical power levels required to heat the WIF wire samples were determined in ground based tests conducted in air at normal gravity, in a vacuum at normal gravity, and in air in reduced gravity aircraft (Learjet) tests. Heating rates that would conserve USML-1 crew time yet maintain nearly uniform insulation temperature were sought. Figure 3 shows plots of temperature versus time for three power

levels (1.22, 1.5, and 1.82 watts), comparing results of the three test environments. The reduced-gravity/air and the normal-gravity/vacuum chamber results were similar for the available aircraft test time. In the vacuum tests, at low heating rates the insulation reached a steady temperature below 100°C where the polyethylene began to melt, while at higher heating rates the temperature rose quickly to excessive temperatures. Temperatures in normal-gravity/air were always lower than the other environments. The vacuum test data were used to specify heater power levels for the WIF flight samples.

Figure 4 shows comparisons of insulation temperatures sensed by thermocouples embedded near the insulation surface as they increased during heating in a quiescent atmosphere then under flow (approximately 10 cm/sec) for three heater power levels (WIF-A,B, and D). In WIF-C, heating in a flow was not performed. Peak temperatures were reached in successively shorter times at higher heater power levels. The heating rates were affected to different extents by the low-speed convection. In the WIF-A and D tests, airflow slowed the heating rate compared to the quiescent case. In WIF-B, the quiescent heating profile is not smooth, suggesting that the heater power was not applied continuously, and the quiescent/convective comparison is difficult. More detailed analysis will be required to complete the comparison of the two environments on wire insulation heating rates.

B. IGNITION AND FLAME SPREADING

Successful ignition of the insulation material was achieved in all four tests. Two of the WIF burning experiments, WIF-A and WIF-C were conducted with flames spreading in concurrent flows, the others, WIF-B and WIF-D, were conducted in opposed flows. Learjet flame spreading tests provided estimates of flame luminosity used to preset the brightness of the thermocouple displays. Generally the WIF flames were much brighter than the flames observed in the Learjet tests, complicating the temperature display observations. The disparity in brightness is attributed to the (sub-atmospheric) cabin pressure in the aircraft in which the experiments were conducted. Additionally, the WIF tests produced surprising amounts of soot, and a molten fuel effect not observable in normal gravity.

C. CONCURRENT FLOW FLAME SPREADING

WIF-A. The first burning test, WIF-A, configured for concurrent-flow conditions, did not ignite on the first attempt. On the second attempt, the igniter was activated for a longer time and the sample ignited. The flame was significantly brighter than the Learjet flame and saturated the video imaging device. The video record shows that as the flame spread, the image brightness pulsated. The pulsations may have been caused by flow velocity fluctuations, however no fluctuations were indicated by the anemometer. The exposure meter in the 35 mm still camera responded quickly enough to these variations to provide

good, clearly resolved exposures. Figure 5 is a black and white reproduction of a single still color frame from the WIF-A flame. A thin blue flame stabilized where the air flow first met the flame, followed immediately downstream a very bright yellow region. The color of the flame gradually changed from the bright yellow to red nearer the downstream flame tip. These visibly luminous regions are associated with thermal radiation from hot soot particles produced in the flame.

The tip of the flame in this concurrent flow case was open, rather than coming to a pointed tip. Soot escaped visibly from the flame, often in large thread-like structures. The overexposed video image precluded quantitative measurements of their length, but fluctuations in the flux of escaping soot particles, apparently in concert with the brightness variations, were observed.

The stabilization region of the flame propagated as the insulation near the flame disappeared from the wire. Normally described as a burnout front, the consumption of fuel in this case combined fuel vaporization and the flow of molten insulation material. The molten material accumulated, forming a continuously growing, quasi-spherical bead two to three times the initial diameter of the insulation (see figure 6). This shape was assumed presumably to achieve a minimum surface energy configuration in the presence of surface tension. The molten bead in the concurrent flow test grew and was not always symmetric with respect to the wire. Near the downstream end of the sample, the gas-phase thermocouple, 1.5 mm from the insulation surface, was occluded by the molten fuel.

Unlike the opposed flow cases described below, the surface of the fuel near the flame in WIF-A, as seen in the still photographs, was discolored and opaque. A gray/brown color persisted throughout the burning time, and was apparently caused by the deposition of soot from the flame onto the surface. In a few of the still photographs, the opaque fuel surface appears to have been fractured or chipped, with an irregularly shaped gap in an otherwise uniformly brown surface. We speculate that a part of the surface soot layer may have been ejected by a bursting vapor bubble.

WIF-C. In the third test, WIF-C, the air-flow was not activated prior to ignition (nor during the heating phase.) A torroidal cloud of vapor or condensed pyrolysis products formed around the igniter and was rendered visible by the scattering of light emitted by the hot ignitor (see figure 7a). Upon reaching a diameter of approximately 30 mm, the cloud ignited suddenly (see figure 7b). The hot gas expansion wave associated with the ignition not only reached but overwhelmed the anemometer flag located 75 mm away.

After the ignition of the cloud the video recording shows an overexposed stationary flame stabilized about the igniter, which also appears to have remained energized (see figure 7c). Over the next several seconds the incipient flame and the hot igniter melted the insulation material in their vicinity, and soot deposition blackened the fuel surface beginning approximately 10 mm from the igniter. The

molten fuel flowed away from igniter, eventually baring the wire between the ignitor and the receding fuel.

Approximately 17 seconds after ignition the GBX air flow was activated. A flame around the igniter became immediately discernible but did not spread beyond the blackened surface downstream. For several seconds the stationary flame bathed the blackened fuel surface which appeared to accumulate soot emitted from the flame and to partially melt and recede an additional 5-6 mm. The flame continued burning until the insulation material near the igniter coil was consumed, approximately 38 seconds after ignition. We speculate that the downstream fuel failed to ignite under the combined effect of oxygen depletion and retarded fuel vaporization, suppressed by the layer of soot on the fuel surface.

D. OPPOSED FLOW FLAME SPREADING

WIF-B. Following ignition, the brightness of the flame in the WIF-B test saturated the video camera, and no structure of the spreading flame is discernible in the video recording. To compensate, Mission Specialist (MS) Carl Meade temporarily extracted the video camera from the GBX while the burn was in progress and reduced the lens aperture to improve the exposure of the spreading flame. The comparative brightness of the thermocouple displays, configured for compatibility with the Learjet flames, was thereby brought below the detection threshold of the video camera for the remainder of the test.

A single frame of this flame is shown in Figure 8. Molten insulation material flowed into an ellipsoidal bead just inside the leading edge of the flame. Approximately 1 mm ahead of the visible flame, a melting front in the virgin fuel is visible in the still photographs, seen as a change from translucence to transparence. A dark surface layer, about 1-2 mm in length, appears near the flame stabilization point. Similar observations have been made of polyethylene material radiatively heated in air in normal gravity, but not when heated in a nitrogen atmosphere. This discoloration may indicate that some degree of oxidative degradation of polyethylene occurred at the fuel surface.

Throughout the opposed flow tests, the flame stabilization region and the accumulation of molten fuel under the flame remained symmetric with respect to the wire axis. The size of the molten bead reached a steady size and shape, as shown in Figure 8, within 15-18 seconds.

The still photographs also showed vapor bubbles in the molten fuel. Evidence of the bursting of these bubbles was more clear in the video recording where small jets of flame briefly deform the flame near or in the flame stabilization region. In some instances these disruptions were accompanied by observations of small satellite flames, presumably burning particles of fuel created as the bubble burst. These disruptive events were the principal perturbations of the spreading flames.

The still photographs resolve the flame shape during a short time window and emphasize any captured perturbations of the flame. The video record emphasizes the average shape, though the source of the flame perturbations (e.g. bursting bubbles) are made more clear. In the video record the side, or visible outer boundary, of the spreading flame seems parallel to the wire (and flow) axis and the tip of the flame is completely open (i.e. the end of the luminous region is perpendicular to the flow direction), while the still photographs show some curvature of the flame tip back toward the fuel surface. The still photos show the fuel ball entirely inside the visible flame while the leading edge of the flame in the video appeared to be stabilized at a point nearly 90° around from the leading edge of the molten fuel ball. These distinctions are all attributed to greater sensitivity of the film to the dim blue portions of the flames.

According to the video record, as the flame reached the end of the fuel sample the side of the flame, previously parallel to the flow direction, diverged downstream (see Figure 9). At the same time the visible flame stabilization region moved forward to the front of the spherical molten fuel ball. In this non-spreading flame, more frequent disruptions were observed, caused by the ejection of material (polyethylene fragments and/or burst vapor bubbles) from the molten fuel ball. We speculate that the higher rate of vapor/fragment production was caused by the accumulation of the energy used earlier for flame spreading. This process continued until the spherical mass of fuel was completely consumed.

WIF-D. The fourth test was also configured for opposed flow conditions and resembled WIF-B in appearance. MS Meade replaced the monochrome video camera used in the previous tests with a color camera and, as before, reduced the lens aperture to eliminate the saturation in the video image. In this case the thermocouple displays remained visible because, although the color array is less sensitive overall than its monochrome counterpart, its color balance was in favor of the displays.

Acting on a suggestion of Professor J.S. T'ien, the WIF investigators decided to obtain a direct comparison between flames in opposed flow and quiescent conditions. When the WIF-D flame had spread nearly to the end of the sample, the air-flow was switched off. Figure 10 shows the ensuing sequence reproduced from the video recording. The visible flame quenched rapidly, receding downstream from the former stabilization region. The remaining polyethylene material cooled and solidified around the wire core in a nearly spherical bead 4-5 mm in diameter, shown near the right-hand end of Figure 11.

E. FLAME SPREAD RATES AND LENGTHS

The 35 mm photographic sequences provided the better resolution of the flame structure, particularly where precise visualization of the leading blue edge of the flame (essentially invisible in the

video record) was needed. Thus while lacking the time resolution of the video record, the still photographs were used to obtain the flame spread rates of tests WIF-A,B, and D. Flame position data from these measurements are shown in Figure 12. We estimate that the error in each position measurement is less than 0.01 cm, which in the propagation of error analysis[5] indicates an uncertainty in the spread rate measurement of less than 0.001 cm/sec. The spread rate results are summarized in Table 1.

F. MICROGRAVITY OPPOSED FLOW.

The measured spread rates for the two opposed-flow cases differ by only 6%, having values of 0.070 and 0.066 cm/sec for WIF-B and WIF-D respectively. Sample heating just prior to ignition (see also Figure 4 B and D) left the insulation temperature higher in the WIF-B test than in the WIF-D test. Higher bulk fuel temperatures reduce fuel preheating requirements and may explain the faster flame spread rate[6].

G. MICROGRAVITY CONCURRENT FLOW.

In concurrent flow, WIF-A, the visible downstream tip of the flame spread at 0.16 cm/sec; while the base of the flame (where the flame is stabilized and the fuel burnout occurs) spread at 0.12 cm/sec. The length of the flame therefore grew slowly throughout the test at about 0.04 cm/sec. Thus even in the extended test time provided by the glovebox this fuel did not reach an equilibrium flame length in a concurrent flow. While steady flame lengths and propagation rates in concurrent flow have been predicted[7] it is not clear what length of WIF-type fuel would be required to observe steady propagation.

H. NORMAL GRAVITY.

Flame spreading tests of the WIF fuel were performed in normal-gravity, ignited either at the sample top or at the bottom, to observe buoyant opposed or concurrent flows (respectively) interacting with the flame. Tests were also conducted in a horizontal configuration. Still photographs and video images were recorded during these tests for direct comparison with the WIF results. The molten fuel frequently dripped in all the normal gravity tests, and the dripped fuel was collected and weighed. A summary of the flame spread rates, averaged over multiple tests, is shown in Table 2.

I. COMPARISON OF CONCURRENT FLOW RESULTS.

The spreading of the flame tip in the upward case was too rapid to measure in the images obtained, i.e. the flame length exceeded the length of the fuel sample within about three seconds. Additionally, small cross currents in the laboratory air perturbed the flame symmetry with respect to the

fuel. The data imply an upward flame spread rate of at least several centimeters per second for samples of this size, compared to the WIF-A result of 0.16 cm/sec. The flame spreading and fuel heating processes were in many ways not comparable to the microgravity concurrent forced-flow case of WIF-A.

The speeds of the fuel burnout front in the normal-gravity upward test and the WIF-A concurrent flow test were similar (0.13 and 0.12 cm/sec, respectively). The molten fuel in the case of the WIF-A experiment accumulated as described above, and the burnout front propagated at a rate controlled by the rates of fuel melting and fuel vaporization. In the normal-gravity upward burning case, however, the burnout front propagation is strongly influenced by dripping, losing approximately 1/3 of the total fuel mass over the entire test. The similar WIF and normal gravity burnout rates therefore appear to be coincidental.

J. COMPARISON OF OPPOSED FLOW RESULTS.

The downward spreading experiments provide a closer comparison between normal-gravity and microgravity spreading. The microgravity spread rate in a low-speed opposed flow, 0.07 cm/sec, is much slower than the normal-gravity spread rate of 0.24 cm/sec. The bright, sooty image of the WIF flames preclude the simple explanation, oxygen deprivation, for the spread rate difference. It is reasonable to infer that the influences of radiative losses, identified in thin fuel flame spreading tests,[1] play a similar role here.

The behavior of the molten fuel seems to contribute to flame spread rates. In normal-gravity tests significant fuel mass dripped from the sample, 1/2 to 3/4 of the original fuel amount. In the several tests conducted, higher downward spread rates correlated with lower amount of fuel lost to dripping. We speculate that in the downward burning case the dripping may have provided an additional forward heat transfer mechanism in which the molten fuel flows downward along and preheats the virgin fuel, some fraction cooling enough to re-solidify. Where more fuel re-solidifies (and does not ultimately drip), more heat is provided to the virgin fuel, enhancing spreading.

In microgravity, that spreading mechanism is absent - all the fuel vaporizes. However, a thermocapillary flow of molten fuel from the vicinity of the flame toward the virgin fuel is conceivable, though not certain. While an appropriate surface tension difference exists between behind the flame and ahead of the flame, without a detailed surface temperature profile it is not clear if the fuel could flow, by capillarity, past the flame leading edge. Surface tension may affect flame spreading in a secondary way by altering the surface area and streamwise length of the mass of vaporizing fuel.

The quenching demonstrated at the end of WIF-D demonstrated the enhancement by convection of flammability for this fuel in microgravity. In ground-based testing of thin fuels, similar enhancements of microgravity flammability have been observed, and flame-spread rates in air are higher in 5-10

cm/sec opposed flows than in either normal gravity or quiescent microgravity conditions.[2,3,4] An analogous reduced-gravity enhancement by convection of flame spread rates is suggested by the WIF-D result.

K. FLAME TEMPERATURES

Temperature histories of the various thermocouples during the burning phase of the WIF tests were obtained from the video record of the temperature displays. Figure 13 shows the temperature histories obtained for the WIF-A and WIF-D experiments. In the WIF-A experiment (concurrent flow flame spreading) the first peak in the gas-phase temperature represents the passage of the flame tip, followed about 20 seconds later by the higher peak of the flame stabilization region. The later gas-phase temperature profile shows, in contrast, the effect of the thermocouple being occluded by the molten ball of fuel. The temperature reported for the melted fuel, about 520°C, is higher than expected and may be influenced by heat conducted along the thermocouple leads from the flame. The highest temperature measured in the concurrent flow flame was 1060°C.

In the WIF-D experiment (opposed flow flame spreading) the first peak in the gas-phase temperature represents the leading edge of the flame where the flame is stabilized in the flow, and is the highest temperature recorded in the test, about 1000°C. The gas-phase temperature dips lower after the initial peak then displays a second and lower peak representing the trailing edge of the flame. The temperature of the insulation shows a rapid rise to the pyrolysis temperature as the flame approaches, remains flat as the fuel vaporizes, then at burnout increases briefly to a high gas-phase temperature.

The temperature data from these experiments provide an opportunity to compare the global characteristics of flames spreading in concurrent and opposed flows in microgravity. Additional analysis of these temperatures has been proposed that will formulate estimates of heat transfer mechanisms in the flame, both in the flame spread direction and between the flame, the insulation and the wire.

L. SOOT AND PARTICULATE PRODUCTION

In all four tests, the bright yellow-orange color of the flames indicate that significant quantities of soot were produced. In the video recordings, soot can be seen escaping from the flame, most prolifically in the opposed-flow tests. In the normal-gravity tests of this material, this visible passing of soot from the flame was not so easily observed, perhaps because gas velocities (buoyant) are much higher than in the WIF tests (forced) at the downstream end of the flames. In normal-gravity tests, though, some soot does escape and can be collected from the plume above the flames.

In the opposed-flow WIF tests, strand-like soot structures, with lengths of approximately 10 cm, were observed downstream of the flame. The overexposure of the video record in WIF-A did not provide

similar quantitative imaging of the soot escaping from the concurrent-flow flame. Soot escaping from each of the flames accumulated on the exit screens of the test modules. The long soot strands observed leaving the opposed-flow flames were visible in the post-flight inspection of those exit screens. These exit screens, shown in figure 14, are noticeably more soot laden than the concurrent case.

Transmission electron microscopic analysis of the primary particles of the soot revealed mean diameters of 31 nanometers in the opposed-flow tests; primaries formed under concurrent flow conditions exhibited a mean diameter of 27 nanometers. These mean diameters differ by less than one standard deviation, and the apparent difference might prove to be statistically insignificant. Primaries formed under conditions of normal gravity exhibit, in comparison, a mean diameter of 13 nanometers. These results are consistent with contemporary microgravity soot measurements made in gaseous diffusion flames in drop towers.

Of additional interest is the discovery of polyethylene particles on the exit screen of module WIF-C. We speculate that these particles, 100 to 200 nanometers in diameter, are from the visible fuel-vapor cloud observed during the quiescent ignition attempt, and were carried downstream and condensed either in transit or by contact with the cold exit screen.

Many small bubbles were visible within the molten region, particularly in the opposed flow cases. Since the boiling temperatures of some polyethylene degradation products (range from C_1 to C_{100} or higher)[8] are much less than the degradation temperature of polyethylene, when the degradation products are formed inside the sample they are immediately superheated and form bubbles. These bubbles grow by accumulation of degradation products through diffusion in the molten polyethylene. When they become sufficiently large and close to the surface, the pressure in the bubbles is sufficient to cause a sudden rupture, ejecting fragments of the molten polyethylene into the gas phase. The ejection of small burning polymer fragments were often observed during the flame spread process.

CONCLUSIONS

The WIF experiment has provided a significant introductory database for electrical wire insulation overheating and burning in a low-speed convecting environment, a database impossible to create in normal gravity.

The analysis of the insulation temperature data, isolated from the wire and gas-phase temperatures, provided a simple observation of convective cooling effects in two of the four tests. We expect, however, that further analysis of the temperature data will yield quantitative convective heat transfer estimates in the low-speed flow regime that is unique to these tests.

The acquired data on flame size, structure, spread rates and temperatures, the behavior of the molten fuel, the soot production phenomena, etc. are instructive, particularly insofar as some aspects of

the observed behavior have not been previously observed. The behavior we have described of the molten fuel, the prodigious production and size of the soot agglomerates, the formation and bursting of fuel vapor bubbles in a spreading flame, and the transient quenching in an abruptly-created quiescent environment are all phenomena seen first in these tests. Among the more quantitative results are the observation that between the concurrent and opposed flow tests, the opposed flow tests propagate slower and produce more soot. As expected from a glovebox experiment program these data are not conclusive; yet they have already provided a stimulation for additional analysis of the existing data. We hope, for example, to extract additional heat transfer estimates from the temperatures observed during flame spreading. We hope that these data will also inspire the development of some modeling effort to clarify some of the unexpected observations.

REFERENCES

1. Bhattacharjee, S., Altenkirch, R.A., and Sacksteder, K.R., "Implications of Spread Rate and Temperature Measurements in Flame Spread Over a Thin Fuel in a Quiescent, Microgravity, Space-Based Environment," *Combust. Sci. Tech.*, 91, pp.225-242, (1993).

2. Olson, S.L., Ferkul, P.V., and T'ien J.S., "Near-Limit Flame Spread Over a Thin Solid Fuel in Microgravity," *Twenty-Second Symposium (International) on Combustion*, the Combustion Institute, pp. 1213-1222, (1988).

3. Olson, S.L., "Mechanisms of Microgravity Flame Spread Over a Thin Solid Fuel: Oxygen and Opposed Flow Effects," *Combust. Sci. and Tech.*, 76, pp. 233-249, (1991).

4. Sacksteder, K.R., and T'ien, J.S., "Buoyant Downward Diffusion Flame Spread and Extinction in Partial-Gravity Accelerations," submitted to the *Twenty-Fifth Symposium (International) on Combustion*, (1993).

5. Press, W.H., Flannery, B.P., Teukolsky, S.A., and Vetterling, W.T., *Numerical Recipes, the Art of Scientific Computing,* Cambridge University Press, pp. 505-506 (1986).

6. Borgeson, R.A., and T'ien, J.S., "Modeling the Fuel Temperature Effect on Flame Spread Limits in Opposed Flow," *Combust. Sci. and Tech.*, 32, pp. 125-136, (1983).

7. Grayson, G.D., Sacksteder, K.R., Ferkul, P.V., and T'ien, J.S., "Flame Spreading Over a Thin Solid in Low Speed Concurrent Flow: Drop Tower Experimental Results and Comparison with Theory," *Microgravity Sci. Technol.*, to appear.

8. Madorski, S.L., *Thermal Degradation of Organic Polymers*, John Wiley and Sons, Chapter 4, 1964.

Table 1. Initial Fuel Temperature, Flame Spread Rates and Flame Lengths in 10 cm/sec Forced Air Flow

Flame Spreading Direction	Insulation Temperature at Ignition	Leading Edge Propagation Speed	Fuel Burnout-Front Speed	Flame Length
Concurrent (WIF-A)	75-85°C	0.16 cm/sec	0.12 cm/sec	1.8-2.6+ cm
Opposed (WIF-B)	80°C	0.070 cm/sec	-	1.8 cm
Opposed (WIF-D)	70°C	0.066 cm/sec	-	1.9 cm

Table 2. Normal Gravity Flame Spreading Results

Flame Spreading Direction	Flame Leading Edge Propagation Speed	Fuel Burnout-Front Speed
Upward	-	0.13 cm/sec
Downward	0.24 cm/sec	0.18 cm/sec
Horizontal	0.14 cm/sec	0.13 cm/sec

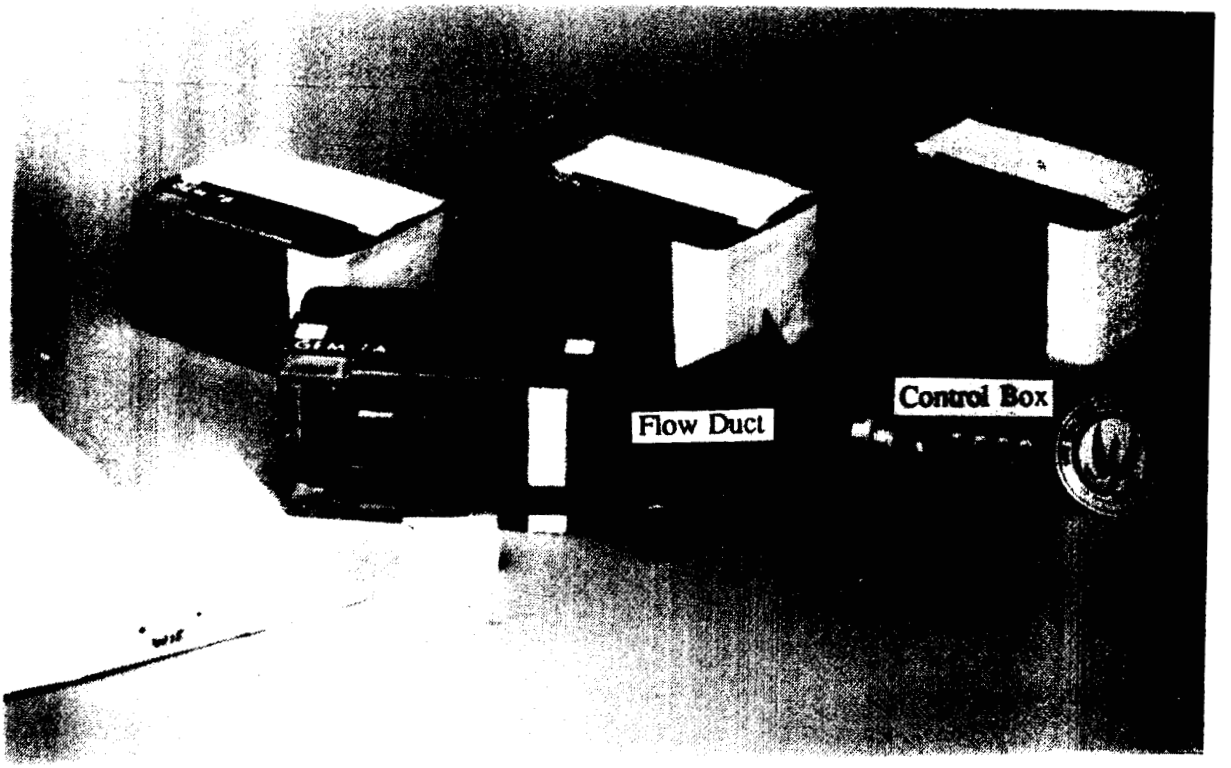

Figure 1 The WIF Flight Hardware.

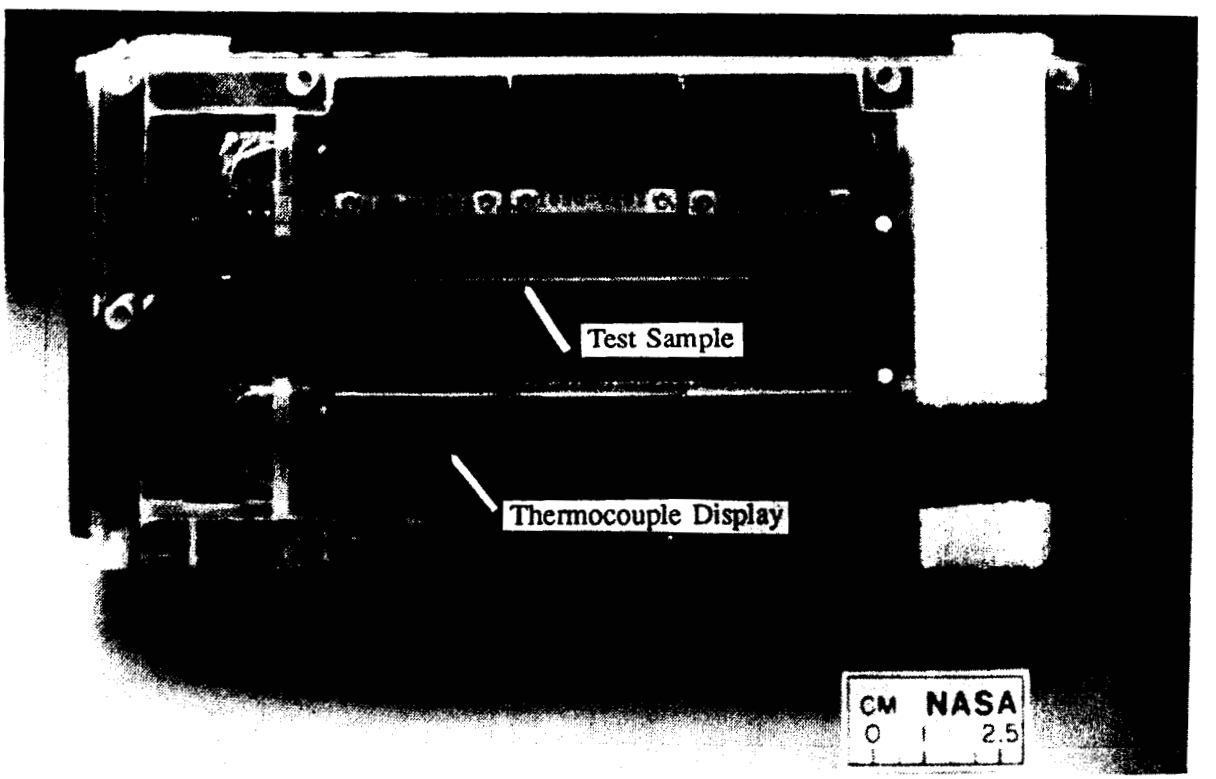

Figure 2 WIF Module: Temperature Displays and Test Sample.

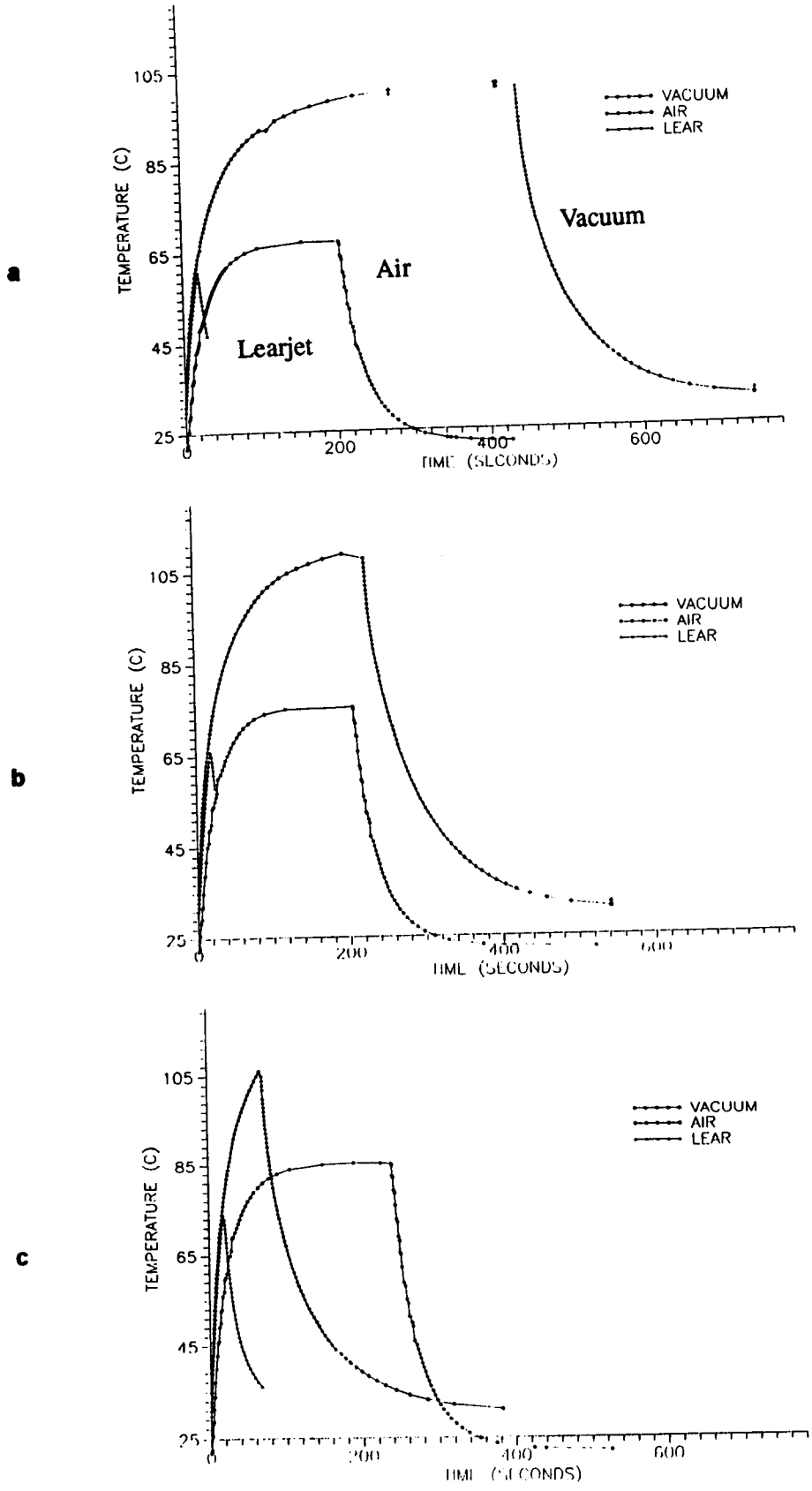

Figure 3 Ground-based wire heating rates, a) 1.22 Watts input power, b) 1.5 Watts input power, c) 1.82 Watts input power.

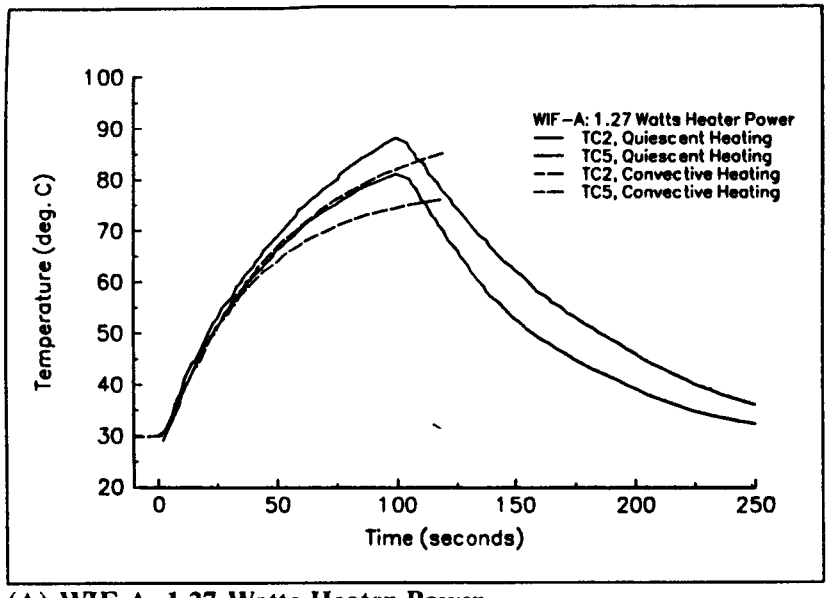

(A) WIF-A, 1.27 Watts Heater Power

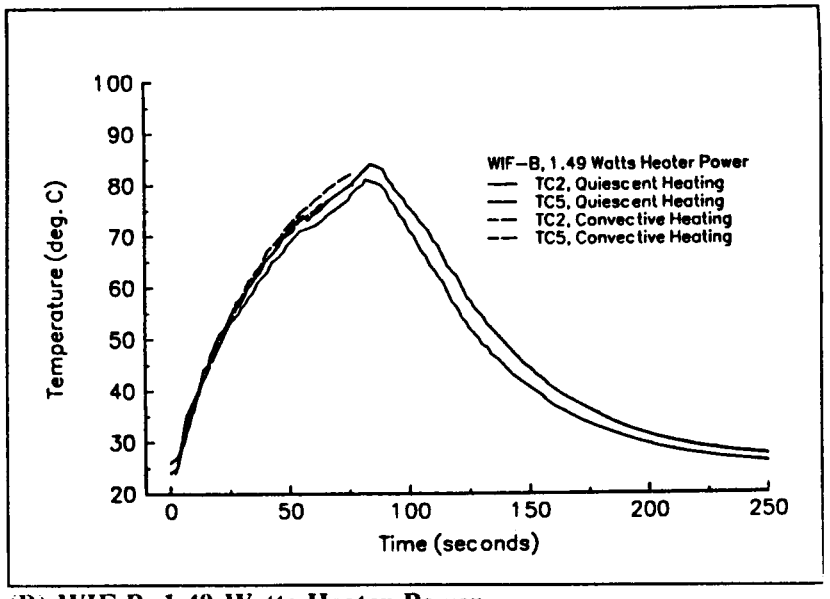

(B) WIF-B, 1.49 Watts Heater Power

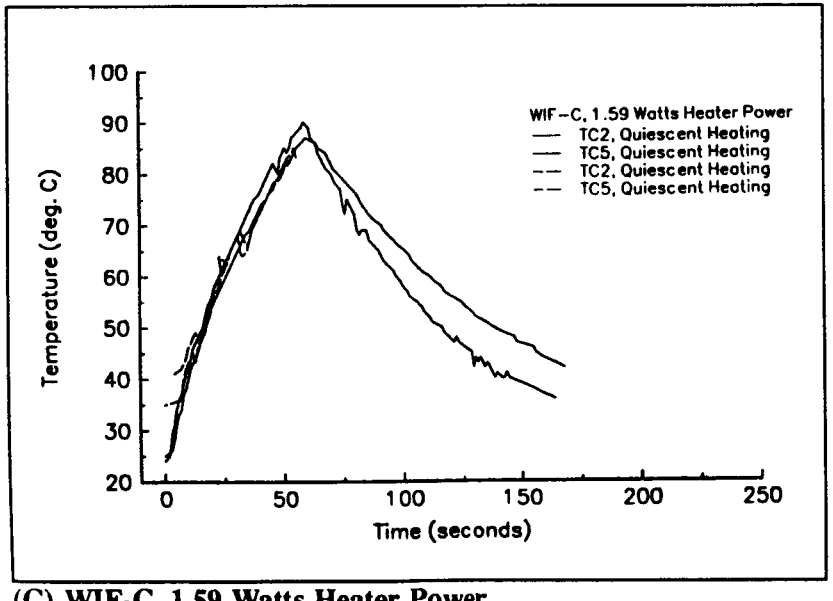

(C) WIF-C, 1.59 Watts Heater Power

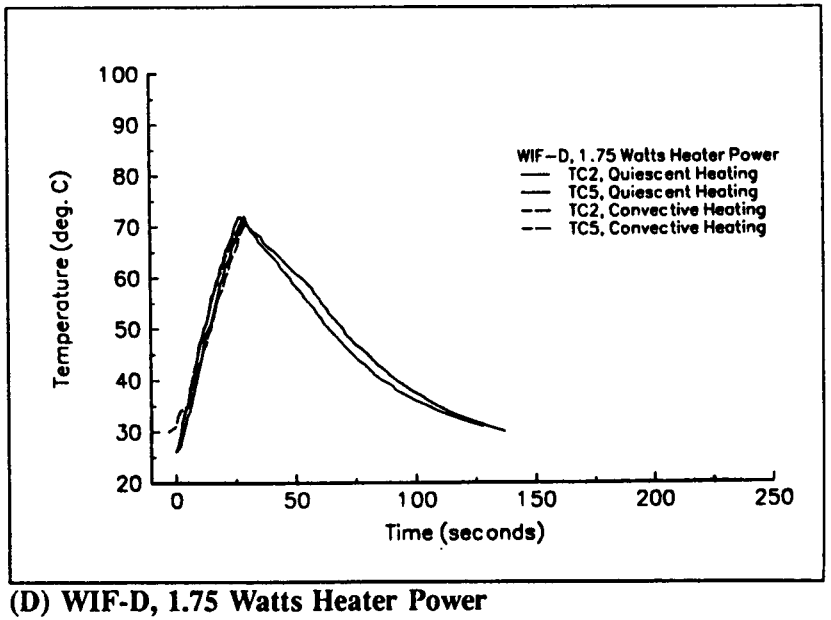

(D) WIF-D, 1.75 Watts Heater Power

Figure 4 Comparison of Quiescent and Convective Heating Rates.

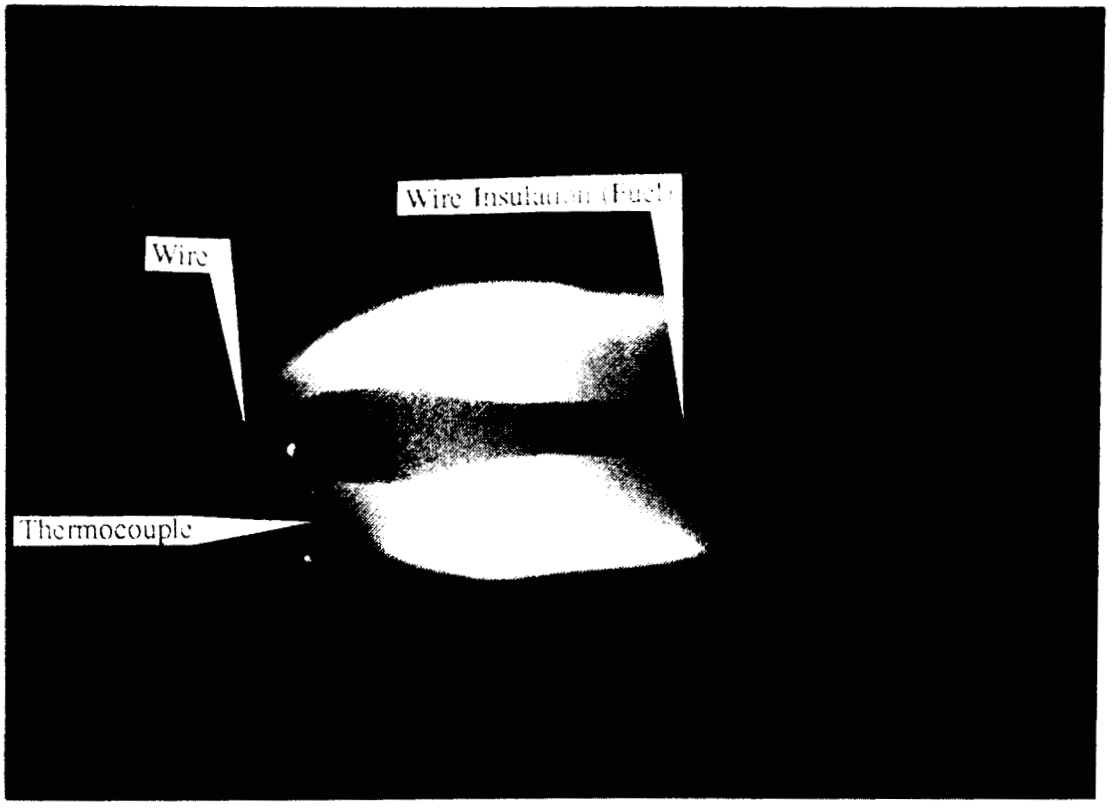

Figure 5 WIF-A, Concurrent Flow Flame; Accumulating Molten-Fuel Bead.

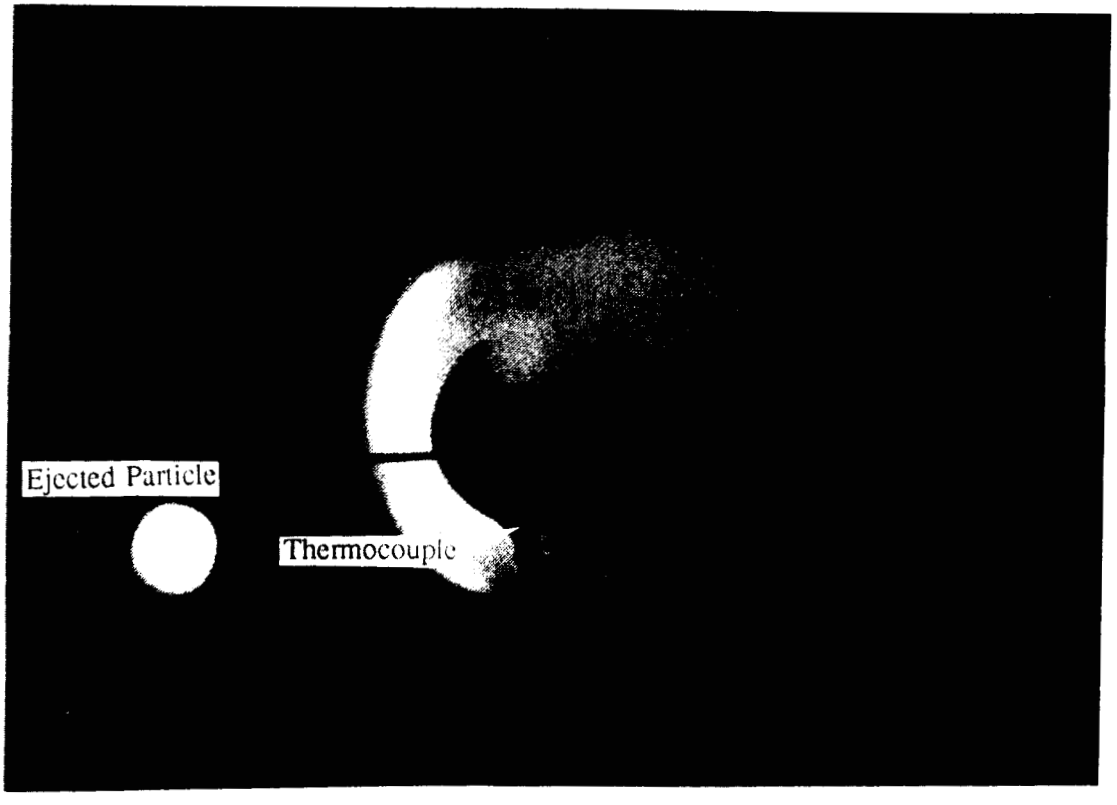

Figure 6 WIF-A, Concurrent Flow Flame; Molten-Fuel Occluding Thermocouple.

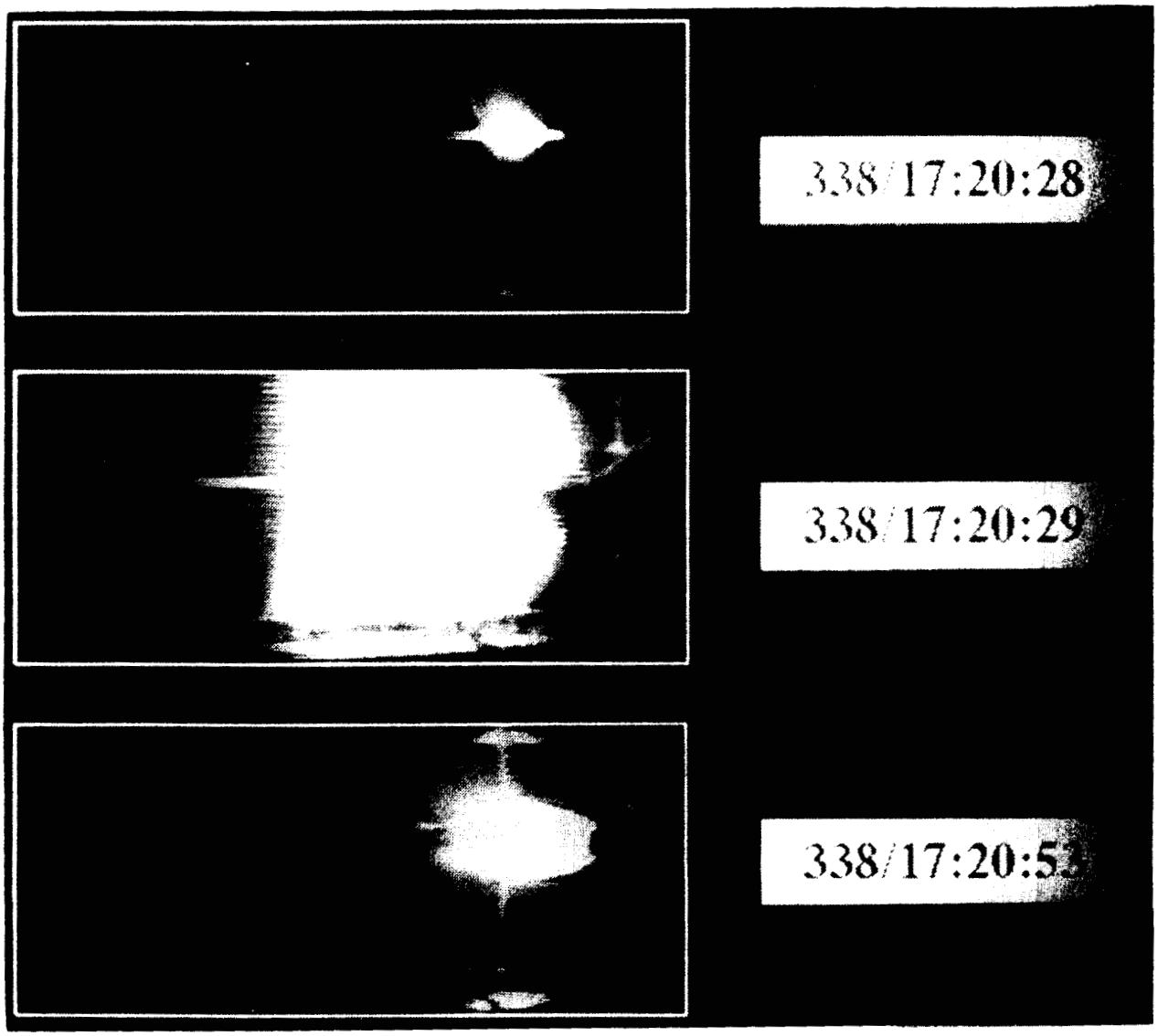

Figure 7 WIF-C, Ignition of Fuel Vapor in Quiescent Air.

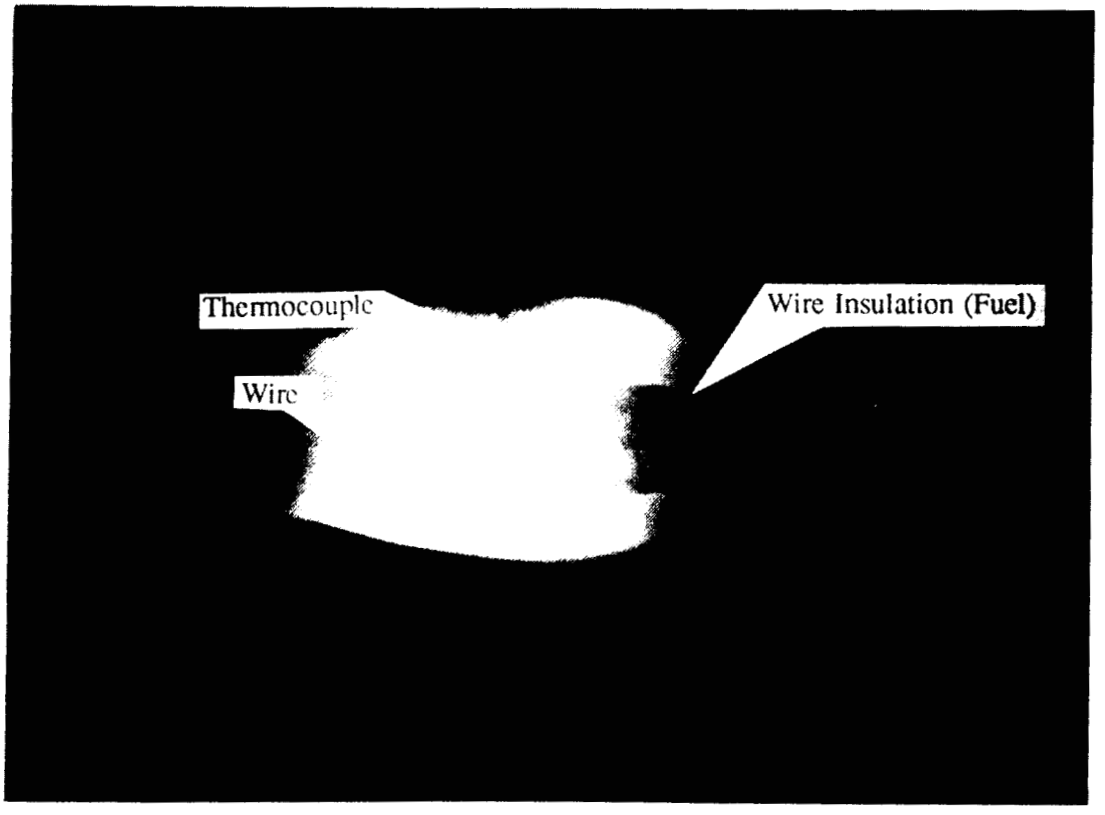

Figure 8 WIF-B, Opposed Flow Flame; Accumulating Molten-Fuel Bead (from Film)

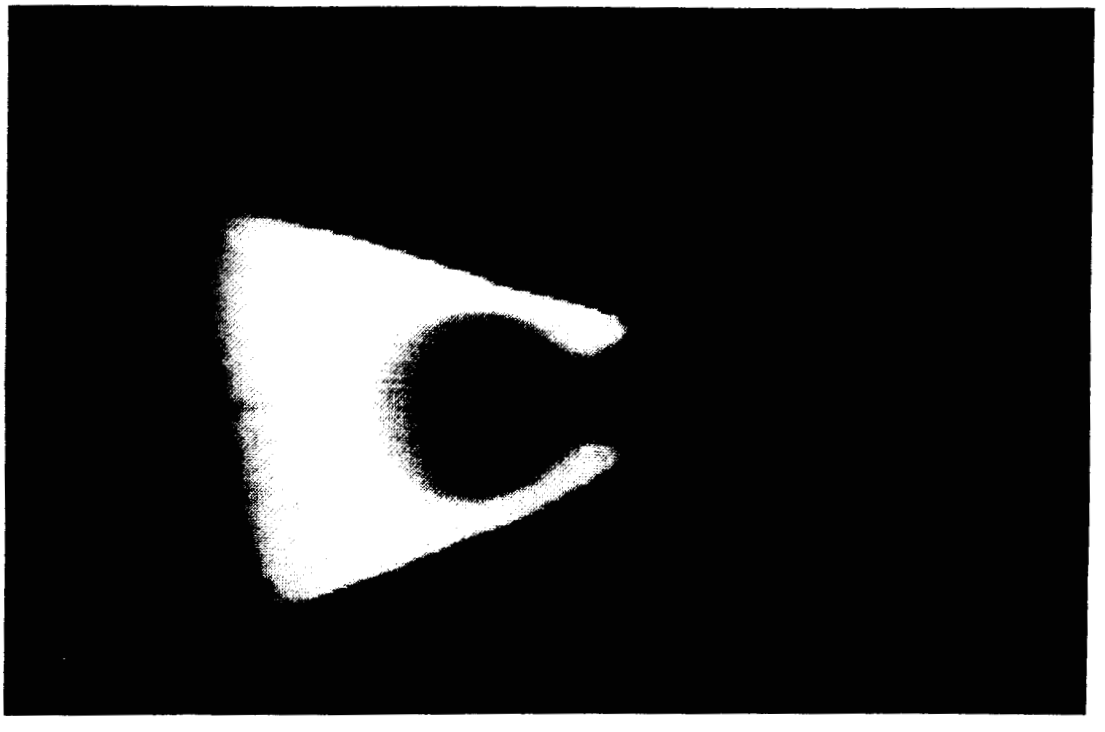

Figure 9 Opposed Flow Flame; Flame Structure at the Fuel End (from Video).

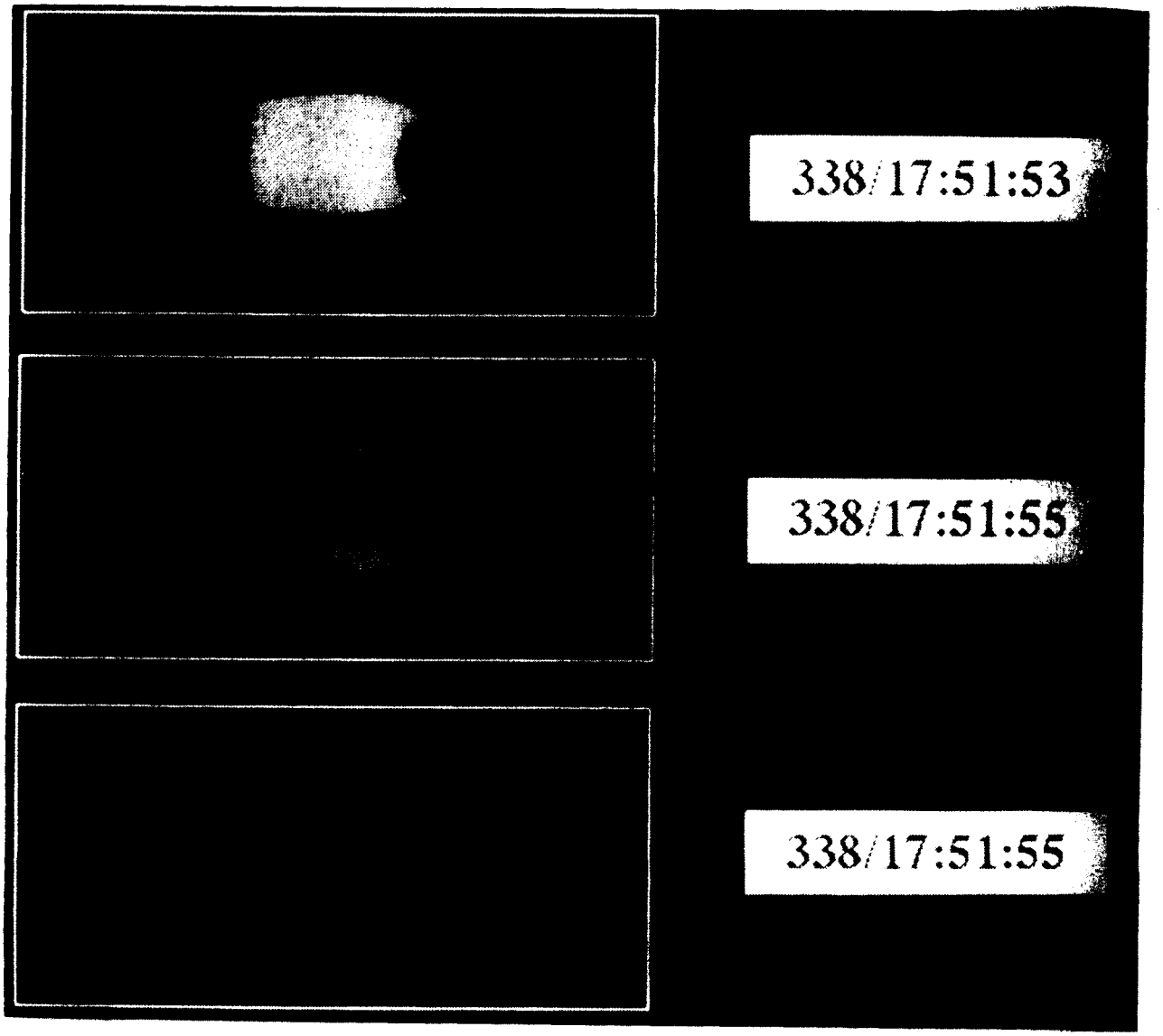

Figure 10 WIF-D, Opposed Flow Flame; Quenching as Flow Stops (from Video).

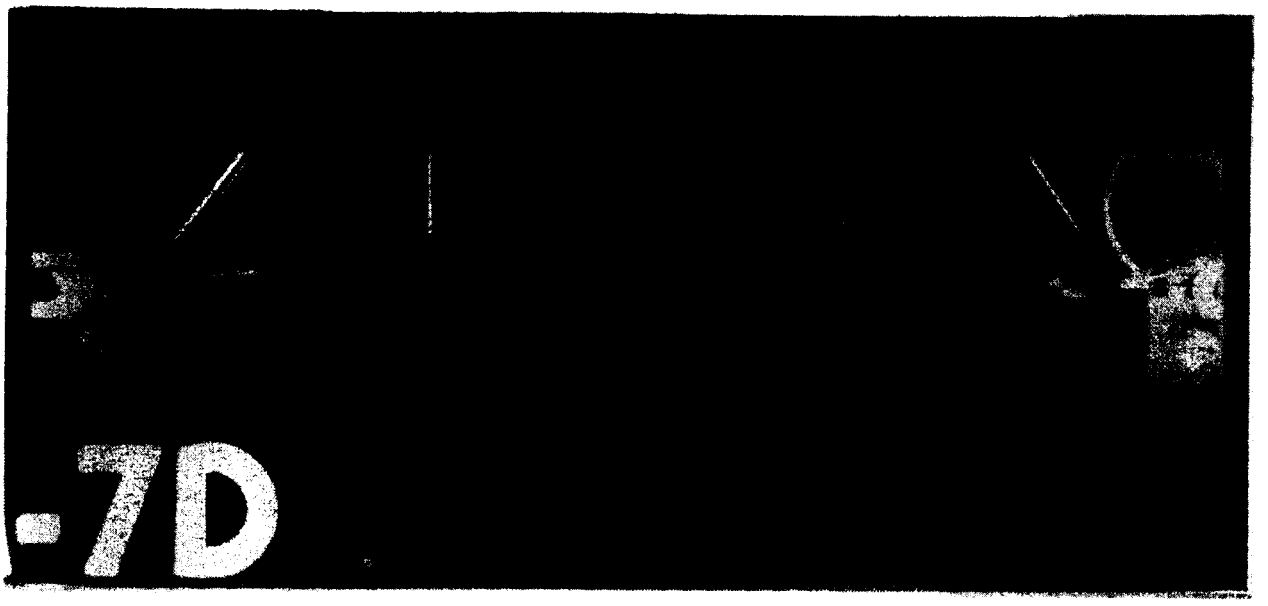

Figure 11 WIF-D, Opposed Flow Flame; Quenched Shape of Molten Fuel (from Film).

a.

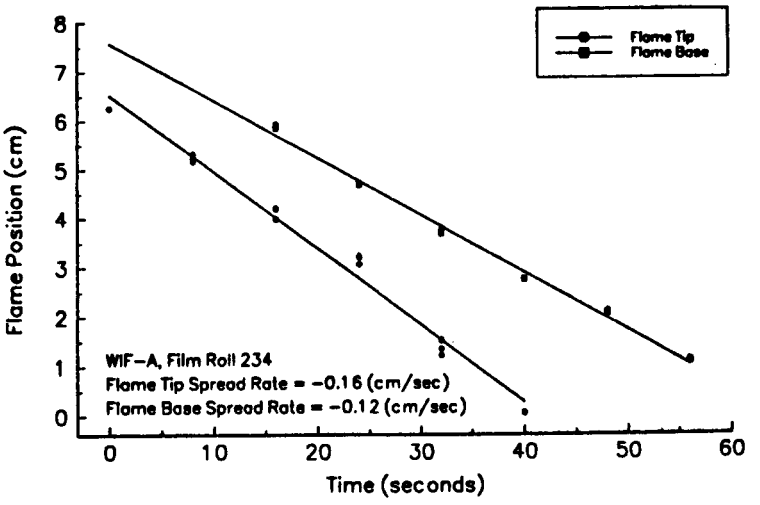

b.

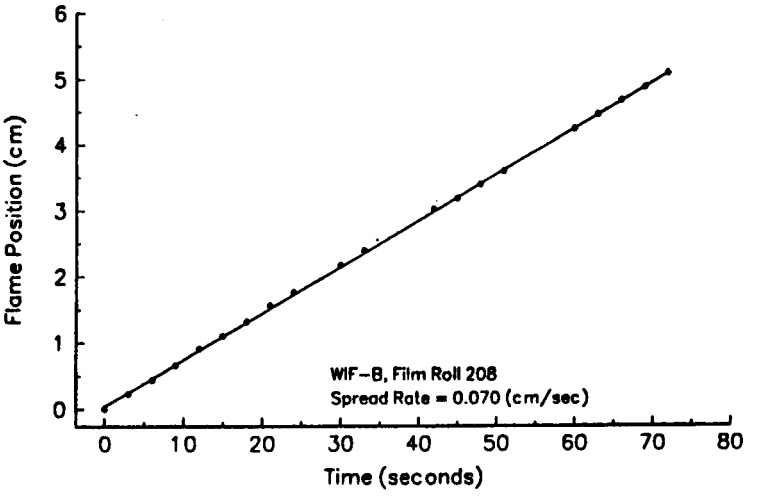

c.

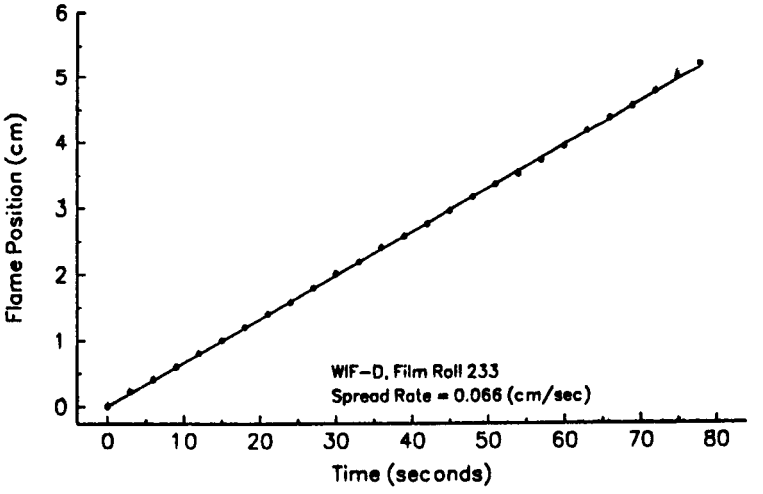

Figure 12 Flame Spread Rate (from film data) a) WIF-A, Concurrent flow flame, b) WIF-B, Opposed flow flame, c) WIF-D, Opposed flow flame.

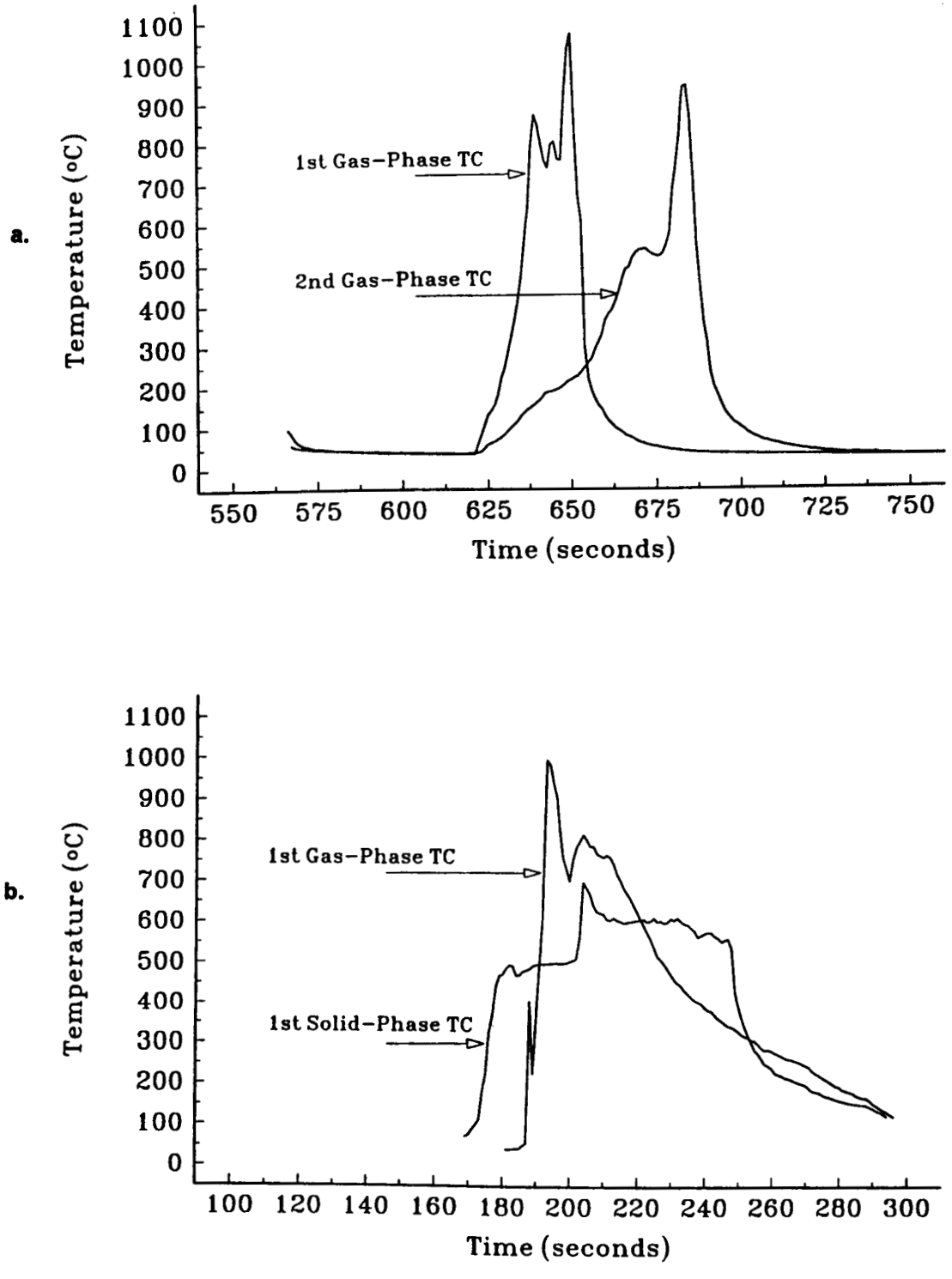

Figure 13 Temperatures during flame spreading, a) WIF-A, Concurrent flow flame, b) WIF-D, Opposed flow flame.

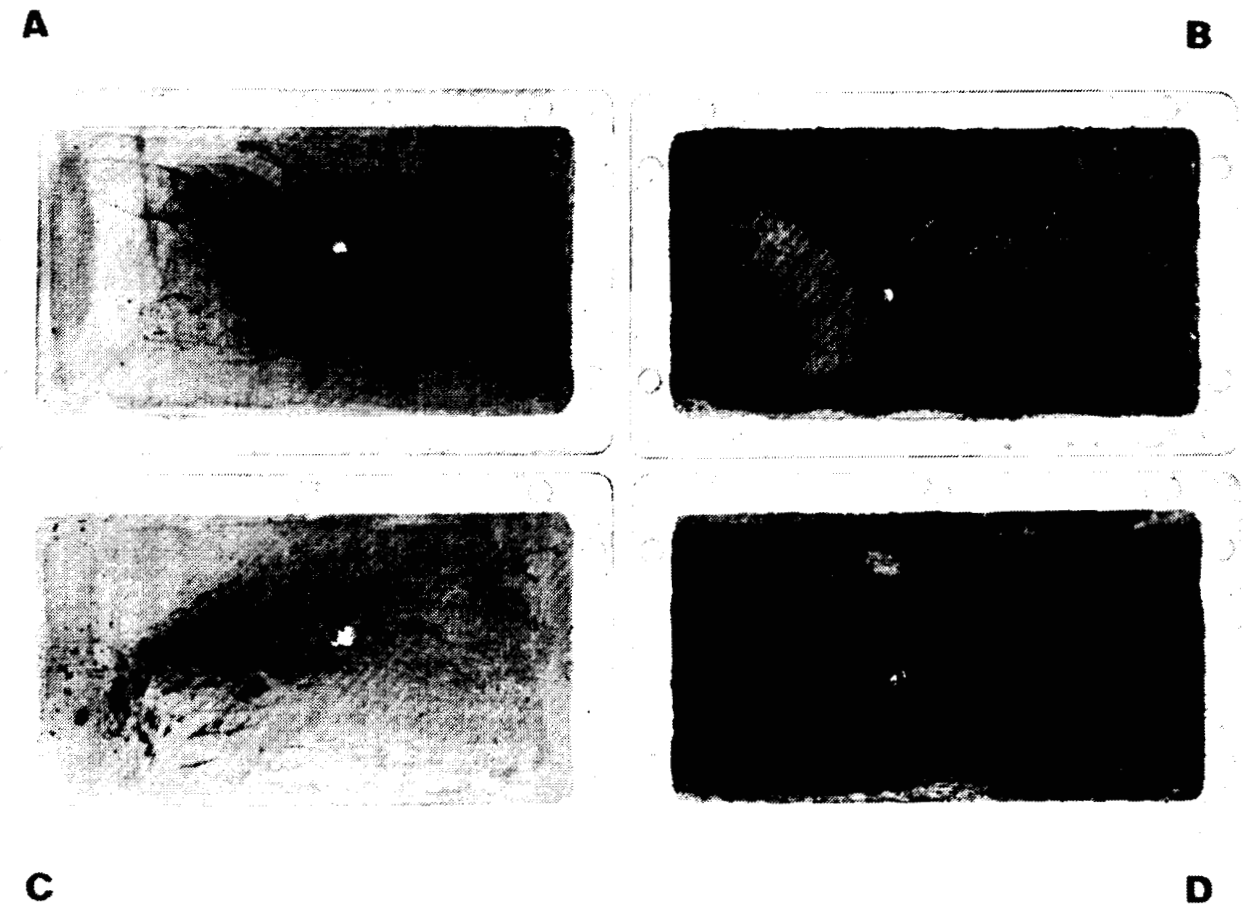

Figure 14 Accumulated Soot on WIF Module Exit Screens.